Published in final edited form as:
Neuron. 2017 August 16; 95(4): 914–927.e4. doi:10.1016/j.neuron.2017.07.020.

Cross-compartmental modulation of dendritic signals for retinal direction selectivity

David Koren[1,2], **James C. R. Grove**[1,3], and **Wei Wei**[1,4,*]

[1]Department of Neurobiology, The University of Chicago, Chicago, Illinois 60637, USA

[2]Interdisciplinary Scientist Training Program, The University of Chicago, Chicago, Illinois 60637, USA

Summary

Compartmentalized signaling in dendritic subdomains is critical for the function of many central neurons. In the retina, individual dendritic sectors of a starburst amacrine cell (SAC) are preferentially activated by different directions of linear motion, indicating limited signal propagation between the sectors. However, the mechanism that regulates this propagation is poorly understood. Here, we find that metabotropic glutamate receptor 2 (mGluR2) signaling, which acts on voltage-gated calcium channels in SACs, selectively restricts cross-sector signal propagation in SACs, but does not affect local dendritic computation within individual sectors. mGluR2 signaling ensures sufficient electrotonic isolation of dendritic sectors to prevent their depolarization during non-preferred motion, yet enables controlled multicompartmental signal integration that enhances responses to preferred motion. Furthermore, mGluR2-mediated dendritic compartmentalization in SACs is important for the functional output of direction-selective ganglion cells (DSGCs). Therefore, our results directly link modulation of dendritic compartmentalization to circuit-level encoding of motion direction in the retina.

eTOC Blurb

Koren et al. find that mGluR2 signaling controls the balance between propagation and compartmentalization of dendritic signals in starburst amacrine cells without affecting local processing within individual dendritic compartments, and directly link this dendritic-level mechanism to retinal direction selectivity.

---

[*]Correspondence: weiw@uchicago.edu.
[3]Present address: Department of Neurobiology, University of California, Los Angeles, California, 90095, USA
[4]Lead Contact

Author contributions
D.K. conducted the experiments in all Figures and the data analysis. J.G. and W.W. conducted experiments in Figures 3 and S4. D.K. and W.W. designed the experiments and wrote the paper.

Keywords

Direction selectivity; retina; electrotonic isolation; mGluR2; motion computation; starburst amacrine

Introduction

Neuronal signaling relies on efficient propagation of synaptic potentials along dendrites, yet spatially restricted propagation between dendritic subdomains often underlies important dendritic computations (Branco and Häusser, 2010). A remarkable example is the dendrites of SACs, which play a central role in generating direction selectivity of DSGCs in the mammalian retina. As an axonless interneuron, the SAC receives glutamatergic inputs from bipolar cells in the proximal dendrites (Vlasits et al., 2016) and releases neurotransmitters GABA and acetylcholine from its distal varicosities (Brecha et al., 1988; Famiglietti, 1991; Kosaka et al., 1988; O'Malley and Masland, 1989; Vaney and Young, 1988) to DSGCs (Figure 1A). The radial branches of a SAC are considered independent computational units that individually prefer centrifugal motion, from the soma to their distal tips (Euler et al., 2002; Hausselt et al., 2007; Miller and Bloomfield, 1983; Velte and Miller, 1997) (Figure 1B). This centrifugal preference has been attributed to multiple cell intrinsic and synaptic mechanisms, including the distribution of active conductances (Euler et al., 2002; Hausselt et al., 2007; Oesch and Taylor, 2010) and chloride transporters (Gavrikov et al., 2003) along the SAC dendrites, proximal targeting of glutamatergic inputs (Vlasits et al., 2016), segregation of excitatory inputs from distinct bipolar cells (Fransen and Borghuis, 2017; Kim et al., 2014; but see Stincic et al., 2016), and lateral inhibition from neighboring SACs and non-SAC amacrine cells (Chen et al., 2016; Ding et al., 2016; Lee and Zhou, 2006).

As distinct computational units, the individual SAC dendritic sectors not only exhibit independent directional tuning to motion stimuli, but also connect to different postsynaptic targets. Each quadrant of the SAC dendritic tree selectively forms inhibitory synapses with one of the four subtypes of On-Off DSGCs whose preferred direction corresponds to the centripetal direction of the SAC quadrant (Briggman et al., 2011; Fried et al., 2002; Lee et al., 2010; Wei et al., 2011) (Figure 1B). Selective wiring between SACs and DSGCs, together with the centrifugal directional preference of SAC dendrites, generates directionally tuned inhibition from SACs to DSGCs during linear motion that is important for the direction selectivity of DSGC spiking output.

Centrifugal direction selectivity of SAC dendritic sectors implies considerable electrotonic isolation between the sectors. Electrical isolation of SAC dendrites has been demonstrated with stationary light flashes: light spatially restricted to one circular sector of a SAC causes local activation without activating other unstimulated sectors (Euler et al., 2002). During linear motion, this is particularly important for reducing the centripetal-direction response of SAC dendrites, since it prevents propagation of depolarization from a centrifugally-stimulated SAC sector to other, weakly stimulated sectors of the same cell.

How is the strong centrifugal response of SAC dendrites generated during full-field motion? One possibility is that it arises solely from local dendritic processing within a SAC sector.

Alternatively, despite considerable electrotonic isolation between SAC sectors, signal integration from multiple dendritic sectors may enhance the response of a centrifugally-stimulated branch due to favorable spatiotemporal summation (Tukker et al., 2004). These possibilities have not been examined experimentally. In the first part of this study, by comparing dendritic responses to motion stimuli crossing the full SAC receptive field with those to motion stimuli spatially restricted to different subfields, we find that multicompartmental signal integration is necessary for the strong and fast centrifugal response during full-field linear motion.

The fine balance between signal isolation and propagation between SAC dendritic sectors shapes the rules of dendritic computation in SACs. However, the regulatory mechanism that sets this balance is completely unknown. A strong molecular candidate is metabotropic glutamate receptor 2 (mGluR2), which is primarily expressed in SACs postsynaptically to bipolar cell synapses, but not in bipolar or ganglion cells (Cai and Pourcho, 1999; Koulen et al., 1996; Seebahn et al., 2008). mGluR2 activation is known to promote neuronal excitability by modulating voltage-gated conductances (Bischofberger and Schild, 1996; Hamlet and Lu, 2016; Ikeda et al., 1995; Knoflach and Kemp, 1998; Kupferschmidt and Lovinger, 2015; Saugstad et al., 1996; Taniguchi et al., 2013) and to influence spiking responses of DSGCs (Jensen, 2006). Nevertheless, the role of mGluR2 in SAC dendritic computation is unknown. In the second part of this study, we find that cross-sector signal propagation, but not local processing within a sector, is altered in the absence of endogenous mGluR2 signaling. This perturbation in SAC dendritic computation impacts the functional output of the circuit, the firing pattern of the direction selective ganglion cells, illustrating the importance of targeted modulation of spatiotemporal dendritic computation for encoding sensory information.

Results

Cross-compartmental signal integration improves the amplitude and latency of the centrifugal response of SAC dendrites during full-field linear motion

To investigate whether the centrifugal response of SAC dendrites during full-field linear motion is generated locally and independently by each dendritic sector, or involves participation from multiple dendritic compartments, we measured the motion-evoked calcium responses of On SAC distal dendrites (Figures 1C and S1) when a moving bar stimulus was delivered to the entire SAC dendritic field, and when it was restricted to different subregions of the field. Stimulation outside the SAC dendritic field did not evoke calcium responses, indicating good spatial control of bipolar cell activation (Figure 1D, outside dendritic field, Figure S2). During full-field stimulation, a large centrifugal response was detected in distal varicosities (Figures 1D and 1E, full field, Supplemental movie 1), consistent with previous studies (Chen et al., 2016; Ding et al., 2016; Euler et al., 2002; Hausselt et al., 2007; Lee and Zhou, 2006; Oesch and Taylor, 2010; Vlasits et al., 2016). During subregion stimulation, we restricted the moving bar stimulus to various subregions of the SAC dendritic field while maintaining a fixed imaging site (Figure 1D). Stimulation restricted to the imaged dendritic sector produced larger responses in the centrifugal direction compared to those in the centripetal direction, indicating that direction selectivity can be computed locally within a dendritic sector (Hausselt et al., 2007) (Figures 1D and 1E, subregions 1 and 2, Supplemental movie 3). However, the amplitude of centrifugally evoked calcium transients during this local stimulation was significantly lower than that during the full-field stimulation (ANOVA $p < 0.0001$), even when the visual stimulus included proximal dendrites that receive most of the excitatory inputs (centrifugal responses in Figures 1D and 1E, full field versus subregion 2; Tukey's post-hoc test $p = 0.0037$). In addition, the onset of the centrifugal response in distal varicosities did not occur until the moving bar reached the distal tips of the dendrites during local stimulation (Figure 1F, subregions 1 and 2), while it occurred when the bar reached the proximal dendrites during full-field stimulation (Figure 1F, full field; ANOVA $p < 0.0001$; Full field vs subregion 2: $p = 0.001$). This enhanced amplitude and faster onset of calcium responses suggest that multicompartmental signal integration plays a role during full-field motion in the centrifugal direction (Fig 1G).

When the moving bar stimulus was restricted to the perisomatic region covering either the proximal 60% of all dendritic sectors (Figure 1D, subregion 3, Supplemental movie 5) or mainly the dendritic sector on the opposite side of the imaging window (Figure 1D, subregion 4, Supplemental movie 6), strong centrifugal responses were readily detected, with an amplitude similar to that during full-field stimulation (Figures 1D and 1E, centrifugal responses of full-field versus subregions 3 and 4). Notably, the responses of varicosities in the imaging window were always stronger during motion in their centrifugal direction, regardless of the spatial extent and position of the subregion motion stimuli (Figures 1E and 1E). Therefore, both trans-somatic signal propagation and local preference of post-somatic dendrites are tuned in the direction of full-field linear motion. This likely presents a physiological advantage for the circuit, because efficient summation of the propagating signal with local excitation improves the amplitude and timing of centrifugal responses (Tukker et al., 2004) (Figure 1G), a computation reminiscent of coincident activation of distal dendrites and perisomatic compartments elsewhere in the nervous system (Bittner et al., 2015; Jarsky et al., 2005; Larkum et al., 2001).

Electrotonic isolation maintains the weak centripetal response of SAC dendrites

In contrast to the strong responses during motion in the centrifugal direction of the imaged dendrites, the response in the centripetal direction is weak under all stimulus conditions (Figure 1D and 1E), consistent with less effective summation of motion-evoked signals in this direction (Tukker et al., 2004). When the motion stimulus was positioned beyond the soma and covered only the distal 60% of the dendrites on the opposite side of a SAC (Figure 1D, subregion 5), calcium responses were evoked with significantly lower fidelity and amplitude in both centrifugal and centripetal directions (Figures 1D and 1E, subregion 5). A small calcium transient was observed in 55% of the trials when this opposite dendritic sector was stimulated in the centrifugal direction of the imaged dendrites and in 17% of the trials when it was stimulated in the centripetal direction. In contrast, the same stimulus reliably evoked stronger and centrifugally-tuned responses in the distal varicosities of the stimulated dendritic sector (Figure 1D, subregion 1). Therefore, the locally generated centrifugal-direction response within a dendritic sector does not propagate efficiently to the opposite, unstimulated sector due to electrotonic isolation between the sectors. This ensures that during full-field motion, the strong centrifugal response of one dendritic sector does not contaminate the weak centripetal response of the opposite sector (Figure 1G).

mGluR2 blockade enhances the centripetal response of SAC dendrites during full-field motion

The importance of electrotonic isolation in minimizing the SAC's centripetal-direction responses prompted us to examine the mechanisms underlying this isolation. Compartmentalized signaling in dendrites has been attributed to interactions between synaptic inputs, active and passive dendritic conductances and dendritic morphology (Harnett et al., 2013; Johnston et al., 1997; Makara et al., 2009; Otsu et al., 2014). However, it is unclear if the electrotonic properties of SAC dendrites can be acutely modulated in adult animals. Therefore, we searched for regulatory mechanisms of SAC dendritic excitability, and identified the SAC-specific mGluR2 signaling (Cai and Pourcho, 1999; Koulen et al., 1996; Seebahn et al., 2008) as a candidate. First, we tested if mGluR2 signaling affects the response of SAC varicosities to full field linear motion. The mGluR2 antagonist LY341495 consistently increased the amplitude of the full-field centripetal-direction response (Figures 2A–2B, S3 and Supplemental Movie 2). In contrast, it did not affect the centrifugal-direction response (Figures 2A and 2B), suggesting that the strong centrifugal-direction response is saturated (Lipin et al., 2015) and cannot be further enhanced by mGluR2 blockade. As a result, the direction selectivity of SAC dendrites during full-field motion is reduced in mGluR2 blockade (Figures 2C and S3).

mGluR2 blockade selectively increases signal propagation between SAC dendritic sectors

The aberrant centripetal-direction response in mGluR2 blockade may be a result of either a general increase in SAC excitability that impacts local processing of individual dendritic sectors, or a selective reduction in electrotonic isolation between the sectors preferring different directions. In order to distinguish between these possibilities, we asked if mGluR2 signaling affects centrifugal direction selectivity within an individual dendritic sector. When the moving bar stimulus was restricted to the local dendritic sector containing the imaged varicosities (Figure 2D), mGluR2 antagonist LY341495 did not alter the highly directional calcium response of these varicosities (Figures 2D–2F, Supplemental movies 3 and 4), indicating that mGluR2 is not required for the intrinsic centrifugal preference generated locally within a SAC dendritic sector. However, when the stimulus was restricted to the sector opposite the imaging window (Figure 2G), mGluR2 blockade improved the fidelity (Figures 2G and 2H, Baseline vs LY341495: $p = 0.01$, Two-way ANOVA) and amplitude (Figures 2G and 2I, $p = 0.0005$, Two-way ANOVA, Supplemental movies 7 and 8) of the trans-somatic calcium response. Therefore, endogenous mGluR2 signaling is important in preventing aberrant propagation of depolarization between SAC dendritic sectors without affecting local computation within the dendritic sector.

Reduced electronic isolation between SAC sectors during mGluR2 blockade is also evident when the motion stimulus is restricted to the perisomatic region covering the proximal dendrites. Under this condition, LY341495 abolished the direction selectivity of varicosity calcium responses by selectively increasing the response to stimulation in the centripetal direction for the imaged dendritic sector (Figures 2J–2L). Since the centrifugal response was unaffected by LY341495 (Figures 2J and 2K), this illustrates that mGluR2 acts to prevent contamination of weakly-activated SAC sectors by the responses of strongly-activated sectors. Therefore, during linear motion, mGluR2 ensures that signals summate efficiently along SACs in the direction of stimulus motion without back-propagating to centripetally-stimulated varicosities (Figure 1G).

mGluR2 signaling inhibits voltage-gated calcium channels in SACs

To understand the molecular mechanism underlying the effect of mGluR2 on electrotonic isolation, we searched for the ion channel targets of mGluR2 signaling in SACs while blocking synaptic transmission in the retina. We found that mGluR2 does not modulate resting membrane properties in SACs (Figures S4A–S4D). Previously, the Kv3 family of voltage-gated potassium channels had been suggested to underlie electrotonic isolation in SACs (Ozaita et al., 2004). However, we found that the cesium-sensitive voltage-gated outward conductance mediated by these channels is not affected by the mGluR2 agonist LY354740 (Figures 3A and 3B).

We next investigated if mGluR2 modulates voltage-gated calcium currents in SACs by performing voltage-clamp recording using a cesium-based internal solution (see methods). During prolonged membrane depolarization to 0 mV, a regenerative transient is triggered due to imperfect space clamp of the thin distal dendrites (Figure 3C). However, the latency and amplitude of the fast initial peak of this transient are highly consistent across trials (Figure 3C, boxed region) and reliably activated during depolarization to over −30 mV (Figures 3D and 3F). This transient is blocked by the nonselective calcium channel blocker cadmium (Figure S4E), or a combination of N- and P/Q-type calcium channel antagonists ω-conotoxin GVIA (CTX, 1 μM) and ω-agatoxin IVA (AgTX, 250 nM, Figure 3C and 3D), consistent with previous reports on the presence of N- and P/Q type calcium channels in rabbit SACs (Cohen, 2001; Lee et al., 2010). Application of LY354740 reversibly inhibits this calcium transient (Figures 3E, 3F and S4F). Furthermore, in the presence of CTX and AgTX or cadmium, application of LY354740 has no effect on the residual currents in SACs (Figures S4E and S4G). These results indicate that mGluR2 inhibits voltage-gated calcium channels, but appears to operate independently of voltage-gated potassium channels.

To determine whether mGluR2 signaling selectively inhibits P/Q-type or N-type calcium channels, we applied AgTX or CTX individually to the bath solution in the presence of synaptic blockers. Application of AgTX significantly reduced the amplitude of the initial calcium transient (Figures 3G and 3H), and also decreased the frequency of regenerative events during prolonged depolarization (Figure S4H), indicating a significant contribution to the calcium transients by P/Q-type calcium channels. Applying LY354740 in the presence of AgTX eliminated the residual AgTX-insensitive calcium transient, indicating mGluR2 signaling inhibits N-type calcium channels (Figures 3G, 3H and S4H). However, application of CTX alone did not change the amplitude of the initial transient, suggesting that blocking N-type calcium channels alone is not sufficient to modulate the suprathreshold regenerative calcium transient (Figures 3G and 3H). Addition of LY354740 in the presence of CTX decreased the CTX-insensitive inward current (Figures 3G and 3H), indicating that mGluR2 also inhibits P/Q-type calcium channels.

We note that mGluR2 blockade does not directly activate synaptic calcium channels in SAC varicosities during the moving bar stimuli used in this study, because the calcium responses during local stimulation of a dendritic sector were not enhanced by mGluR2 antagonist in either the centrifugal or the centripetal directions (Figures 2D–2F). If the mGluR2 antagonist affected synaptic calcium channels by directly activating them, the centripetal response during local stimulation would increase and the direction selectivity of a process would be impaired. We did not observe this, indicating that the mGluR2 does not directly modulate synaptic calcium channels. Instead, mGluR2 plays a highly specific role in dendritic processing of SACs by regulating trans-somatic propagation of motion-evoked activation between dendritic compartments.

mGluR2 blockade leads to enhanced but delayed inhibition onto DSGCs in the preferred direction

To test how mGluR2 blockade impacts the light response of On-Off DSGCs, we performed whole-cell voltage-clamp recordings of DSGC inhibition, which primarily comes from SAC dendrites extending in the null direction of the DSGC (Briggman et al., 2011; Fried et al., 2002; Lee et al., 2010; Wei et al., 2011) (Figure 4A). During full-field motion in the preferred direction of a DSGC, inhibitory postsynaptic currents (IPSCs) are weak because the presynaptic SAC dendritic sector that releases GABA onto that DSGC is minimally activated by motion in the centripetal direction (Figure 4A, left schematic). Since mGluR2 blockade enhances centripetal responses in SAC varicosities due to back-propagation (Figures 2A–2C), we expect that motion in the preferred direction will produce greater GABA release onto DSGCs, albeit with an increased latency (Figure 4A, right schematic). As expected, when LY341495 was applied, the preferred-direction On IPSCs exhibited an enhanced but delayed component (Figures 4B and 4C). The latency of this enhanced component (289 ± 39 ms, for bar speed of 440 μm/s, Figures 4H and S5A) roughly corresponds to the time necessary for the moving bar to travel one SAC dendritic radius (127 ± 17 μm). Also as expected, the null-direction IPSCs were not significantly affected by LY341495 (Figures 4B and S5A), consistent with saturated centrifugal-direction calcium responses in SACs (Figure 2) and saturated null-direction inhibition in DSGCs (Lipin et al., 2015). Consequently, mGluR2 blockade decreases the direction selectivity of DSGC inhibition (Figure 4D). Similar results were obtained when the contrast of the moving bar was reversed (Figures S5B–S5D). This effect is produced by LY341495 acting specifically on mGluR2 in SACs, because the drug has no effect on the strength and timing of IPSCs in mGluR2 knockout mice (Figures S6A–S6G), nor on IPSCs of alpha retinal ganglion cells in wild type mice, a cell type that is not synaptically connected to SACs (Figures S6J and S6K).

Since the timing of sequential activation of opposite SAC sectors during full-field stimulation depends on the speed of a moving stimulus, we tested the effect of mGluR2 blockade at a higher bar speed. We found enhanced preferred-direction inhibitory inputs onto DSGCs and reduced direction selectivity of inhibition similar to those seen during the lower bar speed (Figures 4E–4G). However, the latency of the preferred-direction IPSC peak at this speed was reduced, since the faster moving bar activates opposite sectors more quickly (Figures 4E and 4H, 147 ± 20 ms, for bar speed of 1100 μm/s), equivalent to a spatial offset of ~ 1.3 SAC radius (162 ± 22 μm). Therefore, mGluR2 blockade in SACs selectively increases preferred-direction inhibition onto DSGCs by enabling propagation of dendritic signals between SAC dendritic sectors that are tuned to different motion directions.

mGluR2 blockade reduces DSGC spiking in the preferred direction at higher motion speed

To test if mGluR2 blockade is functionally relevant to the ultimate output of the retinal direction selective circuit, we examined the spiking activity of DSGCs during perfusion of LY341495. We hypothesized that the enhanced but delayed preferred-direction inhibition during mGluR2 blockade decreases DSGC firing rate. Since SACs release both acetylcholine and GABA to DSGCs, we first examined the effect of mGluR2 antagonist on DSGC EPSCs. In contrast to the increased IPSCs, we found no significant change in the peak EPSC or overall excitatory charge transfer during moving stimuli in the presence of LY341495 (Figures 5B and 5C), presumably because centripetally activated SAC dendrites only contribute to a small fraction of the total excitatory inputs onto DSGCs (Figure 5A, also see Discussion). In order for delayed IPSCs to impact DSGC spiking, the two must temporally coincide. Therefore, we compared temporal relationship among the evoked excitatory and inhibitory charge transfer and firing rate of DSGCs. In baseline conditions, inhibitory charge transfer in response to a bar moving at 440 μm/s was delayed by 100–200 ms relative to the excitatory charge transfer (Figures 6A and 6B) consistent with previous studies (Pei et al., 2015; Taylor and Vaney, 2002). The statistically significant effect of LY341495 on IPSCs evoked at this speed began after 70% of the excitatory charge transfer and 77% of DSGC spiking had already occurred (Figure 6B). By contrast, the baseline inhibitory charge transfer in response to a bar moving at 1100 μm/s was coincident with the excitatory charge transfer (Figures 6C and 6D). Because of the reduced latency of the aberrant inhibition at faster stimulus speed, the effect of mGluR2 blockade on IPSCs began after only 49% of the excitatory charge transfer and 59% of DSGC firing had occurred (Figure 6D). Consistently with this result, LY341495 reduced DSGC firing during an 1100 μm/s stimulus, predominantly while IPSCs were increased (Figure 6D); by contrast, there was no statistically significant reduction in DSGC firing during a 440 μm/s stimulus (Figure 6B).

The effect of LY341495 on DSGC firing gradually increased with increasing stimulus speed between 440 μm/s and 1760 μm/s, consistent with a mechanism based on the degree of temporal overlap of EPSCs with enhanced IPSCs (Figure 6E). The mGluR2 antagonist had no effect on DSGC firing rate in the KO mice (Figures S6H and S6I), further validating our pharmacological approach. Together, these data illustrate that the reduction in DSGC firing during mGluR2 blockade is speed-dependent and is due to aberrantly large IPSCs. This indicates that mGluR2-dependent dendritic computation in SACs is particularly important for the generation of strong preferred-direction DSGC spiking at higher motion speed, suggesting a role for mGluR2 signaling in the broad speed tuning of On-Off DSGCs.

Discussion

Our findings highlight the importance of regulated interaction between dendritic subdomains in dendritic computation, even for strongly isolated and functionally distinct dendritic compartments. While many current models assume that centrifugal direction selectivity of SAC dendrites is independently computed within individual dendritic sectors, our results demonstrate that direction selectivity of SAC dendrites during full-field motion arises from the delicate balance between electrotonic isolation and cross-compartmental signal integration. Signal integration from the entire dendritic tree primes and amplifies the response to centrifugal motion, while electrotonic isolation attenuates the response to centripetal motion.

A role for multicompartmental signal integration in the centrifugal direction confirms a prior modeling study that predicted efficient summation in the centrifugal direction at the distal SAC dendrites due to temporal coincidence of local excitation with the “global” signal spreading from the rest of the dendritic tree (Tukker et al., 2004). In contrast, the local signal in the centripetally-stimulated distal dendrites does not coincide with the temporally delayed global signal, leading to little summation. The global signal in the centripetally-stimulated dendrites is highly suppressed by mGluR2-mediated electrotonic isolation, which prevents the subsequent strong activation of the opposite, centrifugally-stimulated sector from back-propagating and contaminating the centripetal response of the original sector.

In our study, neither the centrifugal responses in SAC varicosities nor the resultant null-direction IPSCs in DSGCs were significantly affected by LY341495, illustrating that the SAC centrifugal response is robust to the decrease in multicompartmental integration caused by mGluR2 signaling at our stimulus conditions. This indicates that favored spatiotemporal integration across SAC dendrites is capable of evoking maximal GABA release from SACs at the endogenous level of mGluR2 signaling. This finding is consistent with nonlinearities in the SAC response to whole-field motion demonstrated in previous studies, which found that SAC GABA release and DSGC direction selectivity are saturated for a wide range of stimulus contrasts and speeds (Amthor and Grzywacz, 1991; Grzywacz and Amthor, 2007; Lipin et al., 2015). By contrast, we find that the SAC centripetal response is significantly modulated by mGluR2 signaling, illustrating that dendritic nonlinearities can enable modulation of dendritic responses in a direction-selective manner (Figure 7). However, we cannot rule out that mGluR2-dependent changes in dendritic integration could affect the centrifugal response during other stimulus conditions.

Optimized balance between signal isolation and cross-compartmental integration is subject to neuromodulation via mGluR2 signaling. mGluR2 activation inhibits N- and P/Q-types of voltage-gated calcium channels in SACs. These calcium channels have been shown to participate in synaptic release of acetylcholine and GABA from SACs in the rabbit (Lee et al., 2010). However, when endogenous mGluR2 signaling is blocked, we did not detect an increase in calcium responses during local stimulation within the dendritic sector, indicating that endogenous mGluR2 signaling does not directly inhibit synaptic calcium channels and synaptic transmission under our stimulus conditions. Instead, this mechanism controls a subpopulation of calcium channels specifically involved in trans-somatic signal propagation. This specificity may be a consequence of the segregation of proximal glutamatergic input sites from distal neurotransmitter release sites on SAC dendrites (Vlasits et al., 2016). For example, proximally-localized mGluR2 may gate the trans-somatic propagation of depolarization without affecting depolarization and calcium influx in distal varicosities.

mGluR2-dependent inhibition of voltage-gated calcium channels likely acts in concert with other cell-intrinsic and synaptic mechanisms that are targeted to the proximal dendritic region of the SAC to promote electrotonic isolation between dendritic sectors. These mechanisms include proximal expression of Kv3 channels (Ozaita et al., 2004) and enriched inhibitory inputs onto the proximal dendrites from neighboring amacrine cells (Ding et al., 2016).

Pharmacological blockade of mGluR2 signaling in our study preferentially impact SACs in the direction selective circuit, since mGluR2 expression is mainly restricted to SACs in the rodents (Koulen et al., 1996; Seebahn et al., 2008), and the mGluR2 promoter has been used to drive GFP expression selectively in On and Off SACs in a transgenic mouse line (Watanabe et al, 1998; Wang et al, 2007). Besides SACs, rod amacrine cells, presumably A17 amacrine cells, exhibit weak immunofluorescence for mGluR2 (Koulen et al., 1996; Seebahn et al., 2008). However, lack of mGluR2 in the rod amacrine cells is unlikely to contribute to the effect we observed, since the rod pathway is saturated under the photopic visual stimulus condition in our study. The selective expression pattern of mGluR2 in rodents is in contrast to that in the cat or rabbit, which has been reported to include the horizontal and multiple types of amacrine cells (Cai and Pourcho, 1999; Jensen, 2006).

mGluR2-dependent dendritic computation in SACs is important for the DSGC spiking output that is conveyed from the retina to the brain during preferred-direction motion. This effect appears to rely on speed-dependent coincidence between excitatory and inhibitory inputs. Most GABAergic synapses onto a DSGC arise from SAC dendrites that prefer motion in the null direction of the DSGC. The somata of these SACs are mostly located on the null side of the DSGC. To elicit enhanced IPSCs onto a DSGC during preferred-direction motion in mGluR2 blockade, the stimulus must activate the more distant sectors of these SACs. Therefore, the latency of enhanced IPSCs during mGluR2 blockade depends on the speed of motion. At lower speeds, the increase of IPSC during mGluR2 blockade lags the excitation and spiking, and therefore has little effect on the firing rate of DSGCs. At higher speeds, the mGluR2-dependent change in IPSC occurs with a shorter latency, and overlaps more with the temporal window of excitation and spiking. As a result, mGluR2 blockade exerts a greater impact in DSGC spiking at higher stimulus speeds. While we cannot rule out the possibility that additional mechanisms play a role in reducing DSGC spiking during high-speed motion in mGluR2 blockade, the temporal correspondence of enhanced IPSCs and spiking reduction strongly suggest a causal link.

In addition to GABA release, SACs provide cholinergic excitation to DSGCs. However, mGluR2 blockade has a less noticeable effect in the EPSCs of DSGCs. Several factors may contribute to this result. First, EPSCs of DSGCs contain an mGluR2-insensitive bipolar component. Second, the cholinergic inputs onto DSGCs come from SAC dendrites oriented in all directions, but only the centripetally activated dendrites show increased calcium transients during mGluR2 blockade. Therefore, only a subset of cholinergic inputs onto DSGCs during preferred direction motion could be affected by mGluR2 blockade, while the majority of GABAergic inputs are enhanced by mGluR2 blockade. Third, since acetylcholine release from SACs has been shown to require higher calcium concentration than GABA release (Lee et al., 2010), it is possible that back-propagation during mGluR2 blockade is less efficient in enhancing cholinergic ESPCs compared with GABAergic IPSCs onto DSGCs. Furthermore, even when an increase is detected in the decaying phase of EPSCs at the speed of 1100 um/s, it is insufficient to enhance spiking due to the concomitant increase of IPSC that appears to overturn the excitatory effect.

Endogenous mGluR2 signaling, which is tied to glutamate release, might serve as a safeguard to prevent excess signal propagation across dendritic sectors during strong glutamatergic excitation through ionotropic receptors. Thus, SAC dendrites represent an intriguing example where the dendritic computation algorithm dynamically adjusts to input conditions through activity-dependent neuromodulation. We believe that our study will initiate future studies on the optimization of dendritic computation rules by neuromodulatory systems. A deeper understanding on this topic is important for delineating and modeling input-output relationships of individual neurons and neural networks, and ultimately, to link dendritic processing to behavior.

STAR Methods

CONTACT FOR REAGENT AND RESOURCE SHARING

Further information and requests for resources and reagents should be directed to, and will be fulfilled by the Lead Contact, Dr. Wei Wei (weiw@uchicago.edu).

EXPERIMENTAL MODEL AND SUBJECT DETAILS

Animals—The mGluR2−/− mouse line (B6;129S-Grm2^{tm1Nak}*/NakRbrc)* (Moreno et al., 2011) was a generous gift from Dr. Javier González-Maeso at Virginia Commonwealth University. *Chat-IRES-Cre* mice (129S6-*Chat*$^{tm2(cre)Lowl}$/J) and floxed *tdTomato* mice (129S6-*Gt(ROSA)26Sor*$^{tm9(CAG\text{-}tdTomato)Hze}$/J) were acquired from the Jackson Laboratory. *Drd4–GFP* mice, in which posterior-preferring DSGCs are selectively labeled, were originally developed by MMRRC in the Swiss Webster background, and were subsequently backcrossed to C57BL/6 background. All strains were backcrossed to the *C57BL/6* background in our laboratory, and crossed to each other to create the lines used in this study.

All experiments were performed on healthy mice of normal immune status which had not been previously used for tests or procedures. Mice were housed in 12 hr-12 hr light-dark cycles in groups of 2–5 per cage and were provided with food and water ad libitum. For electrophysiology experiments, mice of ages P21–P40 of either sex were used. All procedures to maintain and use mice were in accordance with the University of Chicago Institutional Animal Care and Use Committee (Protocol number ACUP 72247) and in conformance with the NIH Guide for the Care and Use of Laboratory Animals and the Public Health Service Policy.

METHOD DETAILS

Intravitreal injection of AAV vector—*Chat-IRES-Cre* mice aged P14–25 were anesthetized using 4μL/g intraperitoneal injection of 10% ketamine/5% xylazine in PBS. Animals were placed on their side and the periorbital region was locally anesthetized using one drop of 0.5% proparacaine HCl (Henry Schein, Melville, NY). An insulin syringe was first used to penetrate the cornea lateral to the lateral limbus, and a Hamilton syringe modified for one-handed micro-injection (Borghuis Instruments) was then inserted into the same incision and behind the lens, injecting 1μL of an AAV vector carrying floxed GCaMP6m (University of Pennsylvania Vector Core) into the vitreal space. This procedure was repeated for each eye. Retinas were isolated and imaged at 2–5 weeks following injection.

Whole-mount retina preparation—Mice were dark-adapted for >30 min, anesthetized using isoflurane, and then euthanized by decapitation. Under infrared illumination, retinas were isolated from the pigment epithelium at room temperature in oxygenated Ames' medium (Sigma-Aldrich, St. Louis, MO) for visual stimulation experiments or in artificial cerebrospinal fluid (aCSF) containing 119.0 mM NaCl, 26.2 mM $NaHCO_3$, 11 mM D-glucose, 2.5 mM KCl, 1.0 mM K_2HPO_4, 2.5 mM $CaCl_2$, and 1.3 mM $MgCl_2$ for dual patch clamp recording. Isolated retinas were then cut into dorsal or ventral halves and mounted ganglion-cell-layer-up on top of a 1 mm^2 hole in a small piece of filter paper (Millipore, Billerica, MA). The orientation of the preferred direction (posterior) *of Drd4-GFP* positive neurons was noted for each piece. Retinas were kept in darkness at room temperature in Ames' medium or aCSF bubbled with 95% O_2/5% CO_2 until use (0–8 hr).

Two-photon calcium imaging—GCaMP6 imaging of SAC varicosities was performed as previously described in (Chen et al., 2016). Retinas were placed in oxygenated Ames' media at 32–33°C and screened using a customized two-photon laser-scanning microscope (Bruker Nano Services Division) for expression of GCaMP6 in displaced SACs. GCaMP6 was excited by a Ti:sapphire laser (Coherent, Chameleon Ultra II, Santa Clara, CA) tuned to 920 nm, and the laser power was adjusted to avoid saturation of the fluorescent signal. To enable simultaneous visual stimulation and GCaMP6 fluorescence, a band-pass filter (Semrock, Rochester, MA) was placed on the OLED to pass blue light peaked at 470 nm, while two notched filters (Bruker Nano Surfaces Division) were placed before the photomultiplier tubes to block light of the same wavelength. The objective was a water immersion objective (60x, Olympus LUMPlanFl/IR).

Tissues in which GCaMP expression lacked nuclear exclusion were not used due to concerns about cell health (Chen et al., 2013). Only areas with sparse infection were used, often at the edge of a larger infected region, in order to allow unambiguous determination of the orientation of individual SAC dendrites. Rectangular imaging regions of length 70–180 μm and width 50–120 μm were chosen surrounding the distal tips of the SAC dendrites.

Visual stimulation—A white organic light-emitting display (OLEDXL, eMagin, Bellevue, WA; 800 × 600-pixel resolution, 60 Hz refresh rate) was controlled by an Intel Core Duo computer with a Windows 7 operating system and was presented to the retina at a resolution of 1.1 μm/pixel. Moving bar stimuli were generated by MATLAB and the Psychophysics Toolbox (Brainard, 1997).

In the plane of the retina, the OLED image was centered in the middle of the imaging window, corresponding to the tips of the imaged dendrites. In the perpendicular axis, the OLED image was focused on the photoreceptor layer. Time series of fluorescence were recorded at 30–50 Hz. After an initial 10-second period to allow the retina to adapt to the two-photon laser, moving bars were presented using the OLED. For full-field stimulation, the bars had dimensions of 220 μm × 660 μm and were presented in three trials of eight pseudorandomized directions, moving parallel to their longer dimension. Bars traversed a patch of retina that exceeded the length of the SAC receptive field by at least 150 μm in both directions.

For spatially restricted stimulation, the bars were presented in 5–10 trials of two pseudorandomized directions (centripetal and centrifugal, which were determined by dendrite orientation and verified by responses to full-field stimulation). These bars had dimensions of 132 μm × 660 μm and moved across a circular patch of retina with a diameter of 132 μm. The speed of the bar was 440 μm/s unless otherwise indicated.

Both positive- and negative-contrast moving bars were used. For positive-contrast (‘bright’) bars, the background light intensity was ~600 isomerizations (R*)/rod/s and the stimulus was ~6.5×10^4 R*/rod/s. For negative-contrast (‘dark’) bars, these values were reversed. During two-photon calcium imaging, additional source of light besides the OLED may activate photoreceptors, including the imaging IR laser at 920 nm and the GCaMP6 fluorescence emitted from the stimulated starburst amacrine cells. We consider the contribution of GCaMP6 fluorescence negligible because GCaMP6 was expressed sparsely in isolated SACs and the GCaMP fluorescence was only activated in ~ 10 varicosities at the distal tips of a SAC. The imaging IR laser, which scanned the same imaging windows, increased the background luminance in the imaging window and triggered a transient calcium response in On starburst amacrine cells at the onset of imaging. Because this IR laser-evoked response adapted within 5 seconds, we started OLED stimulation after at least 10 seconds of laser scanning. Due to the scanning laser, the background illumination at the imaging window was higher than that elsewhere in the retina during OLED stimulation. We estimate that the laser causes an equivalent illumination of about 2×10^4 R*/rod/s at 497 nm according to (Euler et al., 2009). At this level of background illumination, the rod pathway has been shown to saturate and the cone pathway mediates the light response (Borghuis et al., 2013).

Imaging analysis—Fluorescence time series were analyzed offline in Prairie View software (Bruker Corporation) using elliptical regions of interest containing individual SAC varicosities. For each imaging window, an elliptical region of interest adjacent to the varicosities but lacking GCaMP6 signal was chosen to record the background fluorescence. During a visual stimulus, a weak background impulse was detected in this region. This background signal was subtracted from fluorescence measurements of the varicosities and was also used to indicate the onset time of the stimulus. For spatially restricted visual stimulation, stimulus timing was reported by a coincident voltage pulse triggered by MATLAB and recorded by Prairie View software. Responses were background-subtracted, normalized to baseline, clipped, sorted by motion direction and averaged using Microsoft Excel and custom-written MATLAB scripts. The peak amplitude of the averaged responses to each stimulus was calculated as the maximum three-frame running average of $\Delta F/F_0$ during a 2-second period following stimulus onset, where F_0 = the mean fluorescence during the 2-second period before the stimulus and $\Delta F = F - F_0$. The time-integral of the responses was estimated as the right-sided Riemann sum of $\Delta F/F_0$ beginning at stimulus onset and ending 4 seconds later.

For stimuli that did not consistently evoke responses (those localized outside the SAC receptive field or to distant SAC dendritic sectors), a threshold of $F_0 + 3*S.D.$ was applied to the averaged response of identified varicosities within the imaging region to determine whether a response occurred, where S.D. = standard deviation of the region of the ΔF trace in the 2-second period before the first stimulus. Response probability was calculated by dividing the number of evoked suprathreshold responses by the number of trials (5–10). To exclude rare spontaneous calcium events, only responses beginning in the 2 seconds following stimulus onset were considered evoked.

The retinal location of the stimulus during response onset was estimated by multiplying the latency to the response threshold by the speed of the bar. Due to the delays inherent in phototransduction, calcium influx, and GCaMP6m activation, GCaMP6m signal onset may be expected to lag behind the bar. This lag was estimated by presenting a stationary spot of radius 50 μm that was synchronized with the fluorescence time-series acquisition. The measured latency to fluorescence onset was approximately 50 ms. For a bar moving at 440 μm/s, this corresponds to a lag of 22 μm on the retina.

To assess direction selectivity of SAC distal dendrites, we used the direction selectivity index (DSI), defined as $\frac{\Delta Fcf - \Delta Fcp}{\Delta Fcf + \Delta Fcp}$, where ΔF_{cf} is the relative fluorescence change in centrifugal motion and ΔF_{cp} is that in centripetal motion. For statistical analysis, we compared variance across varicosities on the dendrites of the same SAC versus variance across varicosities of different SACs. Since the latter was larger, we averaged DSI of all the varicosities belonging to one SAC to get a single data point, and took N in the statistical analysis to be the number of cells, which equals the number of imaging windows.

Cell targeting for electrophysiology—Cells were visualized with infrared light (920 nm) and an IR-sensitive video camera (Watec). For experiments using visual stimulation, DSGCs were targeted with the aid of two-photon microscopy in *Drd4-GFP* mice. Cell identity was confirmed physiologically by extracellular recordings of responses to moving bars or anatomically using internal solution containing 25 μM Alexa 594 to show the distinctive bistratified dendritic morphology in the SAC sublamina of the inner plexiform layer. For recordings without visual stimulation, SACs and DSGCs were targeted using epifluorescence (X-Cite) in retinas from mice expressing *Chat-IRES-Cre*, floxed *tdTomato*, and *Drd4-GFP*. In these mice, SACs selectively express tdTomato while posterior-preferring DSGCs express GFP. Cell identity was confirmed physiologically by the presence of dual excitatory and inhibitory transmission from SACs to DSGCs.

Alpha cells were identified by their uniquely large size (diameter ≥20μm) and characteristic sustained IPSCs during visual stimulation (van Wyk et al., 2009).

Electrophysiology recording and data analysis—Data were acquired using PCLAMP 10 recording software and a Multiclamp 700B amplifier (Molecular Devices, Sunnyvale, CA), low-pass filtered at 4 kHz and digitized at 10 kHz. Light-evoked responses were recorded at a bath temperature of 32–33°C. Paired SAC-DSGC and SAC depolarization step experiments were performed at room temperature.

For whole-cell recordings, recording electrodes of 2.5–4 MΩ were backfilled with a cesium-based internal solution containing (from Sigma): 110 mM $CsMeSO_4$, 2.8 mM NaCl, 4 mM EGTA, 5 mM TEA-Cl, 4 mM adenosine 5′-triphosphate (magnesium salt), 0.3 mM guanosine 5′-triphosphate (trisodium salt), 20 mM HEPES, 10 mM phosphocreatine (disodium salt), 5 mM N-Ethyllidocaine chloride (QX314), pH 7.25. To preserve potassium channel activity in SACs, $CsMeSO_4$ was replaced by 110 mM $KMeSO_4$ and TEA-Cl was excluded. For whole-cell voltage clamp recordings of SACs, synaptic blockers (from Tocris): 0.008 mM DHβE, 0.05 mM D-AP5, 0.05 mM DNQX disodium salt, and 0.005 mM L-AP4 were applied to the bath solution to block synaptic transmission in the retina. For loose cell-attached recordings, electrodes were backfilled with Ames' media.

Light-evoked IPSCs in DSGCs were isolated by holding cells at 0 mV. Three repetitions of raw synaptic traces were recorded and averaged to obtain the mean response for each stimulus condition and analyzed using PCLAMP 10 software. The peak amplitude and total charge transfer of IPSCs evoked by the On edge of the moving bar (the trailing edge in dark bars) were used to calculate the direction selective index (DSI) and vector sum. DSI is defined as $\frac{P-N}{P+N}$, where P is the peak amplitude or charge transfer of IPSCs in the preferred direction, and N is that in the null direction. Reported potentials have been adjusted for a 10 mV liquid junction potential.

Data from loose cell-attached recordings were analyzed using custom protocols in MATLAB. The number of spikes evoked by the On (trailing) edge of the bar was counted using MATLAB and averaged across trials in each direction. Spike count was quantified in place of spike DSI because the low spike count in mGluR2 blockade reduced the reliability of DSI calculations (Carandini and Ferster, 2000).

Analysis of SAC membrane currents—Outward currents in response to 20-ms depolarization steps in K-based internal were measured by averaging current between 10 and 20 ms during the step. Inward currents in response to depolarization steps in Cs-based internal were measured by first fitting the first 1–6 ms during the step with an exponential function, and then subtracting the peak inward current from the fitted curve. During SAC pharmacological experiments, series and membrane resistance were monitored continuously by including a 5 mV hyperpolarizing step in each sweep. Cells were discarded or experiments were discontinued if their series resistance increased by more than 20% during the recording or exceeded 40 MΩ.

Pharmacology—For light response recordings, 50–100 nM LY341495 (Tocris) was added to Ames' media after baseline experiments. At these concentrations, LY341495 is selective for Group II mGluRs (Kingston et al., 1998). Notably, mGluR3 has not been found in the mammalian retina (Brandstätter et al., 1998). For paired recordings and SAC pharmacology studies, the aCSF was perfused with 500nM-1μM LY354740 (Tocris), a highly selective Group II mGluR agonist (Schoepp et al., 1997) after whole-cell recording was established, and 3 μM LY341495 was subsequently used to competitively inhibit mGluR2 activity

(Kingston et al., 1998). To block voltage-gated calcium channels, 300 μM $CdCl_2$ (Sigma) or combinations of 1 μM ω-conotoxin GVIA (Abcam) and 250 nM ω-agatoxin IVA (Alomone) were added to the aCSF.

QUANTIFICATION AND STATISTICAL ANALYSIS

The number of experimental repeats and sample means ± s.e.m. are indicated in figure legends. In most cases, analysis of calcium imaging movies was performed blind to the mGluR2 antagonist condition. Statistical comparisons were performed using Wilcoxon signed rank test for paired samples or ANOVA followed by post hoc tests (either two-tailed paired Student's *t*-test or Tukey's test, as indicated in figure legends). Repeated measures ANOVA was used in Figures 3B and 3F. $P < 0.05$ was considered significant. * $p < 0.05$; ** $p < 0.01$; *** $p < 0.001$.

DATA AND SOFTWARE AVAILABILITY

The custom MATLAB scripts used for visual stimulation and data analysis are available upon request from the Lead Contact.

Supplementary Material

Refer to Web version on PubMed Central for supplementary material.

Acknowledgments

We thank Chen Zhang for managing mouse colony and intravitreal injections, Dr. Javier González-Maeso at Virginia Commonwealth University for the generous gift of the *mGluR2−/−* mouse line, and the Genetically-Encoded Neuronal Indicator and Effector (GENIE) Project and the Janelia Research Campus of the Howard Hughes Medical Institute GENIE Program and the Janelia Research Campus, specifically Vivek Jayaraman, Ph.D., Douglas S. Kim, Ph.D., Loren L. Looger, Ph.D., Karel Svoboda, Ph.D. for the AAV-GCaMP6 vectors. This work was supported by NIH R01 EY024016, E. Matilda Ziegler Foundation Grant, Sloan Research Fellowship, Karl Kirchgessner Foundation Grant to W.W. and NIH F30EY025958 to DK. The authors declare no competing financial interests.

References

Amthor FR, Grzywacz NM. Nonlinearity of the inhibition underlying retinal directional selectivity. Vis Neurosci. 1991; 6:197–206. [PubMed: 2054323]

Bischofberger J, Schild D. Glutamate and N-acetylaspartylglutamate block HVA calcium currents in frog olfactory bulb interneurons via an mGluR2/3-like receptor. J Neurophysiol. 1996; 76:2089–2092. [PubMed: 8890318]

Bittner KC, Grienberger C, Vaidya SP, Milstein AD, Macklin JJ, Suh J, Tonegawa S, Magee JC. Conjunctive input processing drives feature selectivity in hippocampal CA1 neurons. Nat Neurosci. 2015; 18:1133–1142. [PubMed: 26167906]

Borghuis BG, Marvin JS, Looger LL, Demb JB. Two-Photon Imaging of Nonlinear Glutamate Release Dynamics at Bipolar Cell Synapses in the Mouse Retina. J Neurosci. 2013; 33:10972–10985. [PubMed: 23825403]

Brainard DH. The Psychophysics Toolbox. Spat Vis. 1997; 10:433–436. [PubMed: 9176952]

Branco T, Häusser M. The single dendritic branch as a fundamental functional unit in the nervous system. Curr Opin Neurobiol. 2010; 20:494–502. [PubMed: 20800473]

Brandstätter JH, Koulen P, Wässle H. Diversity of glutamate receptors in the mammalian retina. Vision Res. 1998; 38:1385–1397. [PubMed: 9667006]

Brecha N, Johnson D, Peichl L, Wässle H. Cholinergic amacrine cells of the rabbit retina contain glutamate decarboxylase and gamma-aminobutyrate immunoreactivity. Proc Natl Acad Sci U S A. 1988; 85:6187–6191. [PubMed: 3413087]

Briggman KL, Helmstaedter M, Denk W. Wiring specificity in the direction-selectivity circuit of the retina. Nature. 2011; 471:183–188. [PubMed: 21390125]

Cai W, Pourcho RG. Localization of metabotropic glutamate receptors mGluR1alpha and mGluR2/3 in the cat retina. J Comp Neurol. 1999; 407:427–437. [PubMed: 10320222]

Carandini M, Ferster D. Membrane potential and firing rate in cat primary visual cortex. J Neurosci. 2000; 20:470–484. [PubMed: 10627623]

Chen Q, Pei Z, Koren D, Wei W. Stimulus-dependent recruitment of lateral inhibition underlies retinal direction selectivity. Elife. 2016; 5

Chen TW, Wardill TJ, Sun Y, Pulver SR, Renninger SL, Baohan A, Schreiter ER, Kerr RA, Orger MB, Jayaraman V, et al. Ultrasensitive fluorescent proteins for imaging neuronal activity. Nature. 2013; 499:295–300. [PubMed: 23868258]

Cohen ED. Voltage-gated calcium and sodium currents of starburst amacrine cells in the rabbit retina. Vis Neurosci. 2001; 18:799–809. [PubMed: 11925015]

Ding H, Smith RG, Poleg-Polsky A, Diamond JS, Briggman KL. Species-specific wiring for direction selectivity in the mammalian retina. Nature. 2016; 535:105–110. [PubMed: 27350241]

Euler T, Detwiler PB, Denk W. Directionally selective calcium signals in dendrites of starburst amacrine cells. Nature. 2002; 418:845–852. [PubMed: 12192402]

Euler T, Hausselt SE, Margolis DJ, Breuninger T, Castell X, Detwiler PB, Denk W. Eyecup scope--optical recordings of light stimulus-evoked fluorescence signals in the retina. Pflugers Arch. 2009; 457:1393–1414. [PubMed: 19023590]

Famiglietti EV. Synaptic organization of starburst amacrine cells in rabbit retina: analysis of serial thin sections by electron microscopy and graphic reconstruction. J Comp Neurol. 1991; 309:40–70. [PubMed: 1894768]

Fransen JW, Borghuis BG. Temporally Diverse Excitation Generates Direction-Selective Responses in ON- and OFF-Type Retinal Starburst Amacrine Cells. Cell Rep. 2017; 18:1356–1365. [PubMed: 28178515]

Fried SI, Münch TA, Werblin FS. Mechanisms and circuitry underlying directional selectivity in the retina. Nature. 2002; 420:411–414. [PubMed: 12459782]

Gavrikov KE, Dmitriev AV, Keyser KT, Mangel SC. Cation--chloride cotransporters mediate neural computation in the retina. Proc Natl Acad Sci U S A. 2003; 100:16047–16052. [PubMed: 14665697]

Grzywacz NM, Amthor FR. Robust directional computation in on-off directionally selective ganglion cells of rabbit retina. Vis Neurosci. 2007; 24:647–661. [PubMed: 17900380]

Hamlet WR, Lu Y. Intrinsic plasticity induced by group II metabotropic glutamate receptors via enhancement of high-threshold KV currents in sound localizing neurons. Neuroscience. 2016; 324:177–190. [PubMed: 26964678]

Harnett MT, Xu NL, Magee JC, Williams SR. Potassium Channels Control the Interaction between Active Dendritic Integration Compartments in Layer 5 Cortical Pyramidal Neurons. Neuron. 2013; 79:516–529. [PubMed: 23931999]

Hausselt SE, Euler T, Detwiler PB, Denk W. A dendrite-autonomous mechanism for direction selectivity in retinal starburst amacrine cells. PLoS Biol. 2007; 5:e185. [PubMed: 17622194]

Ikeda SR, Lovinger DM, McCool BA, Lewis DL. Heterologous expression of metabotropic glutamate receptors in adult rat sympathetic neurons: Subtype-specific coupling to ion channels. Neuron. 1995; 14:1029–1038. [PubMed: 7538309]

Jarsky T, Roxin A, Kath WL, Spruston N. Conditional dendritic spike propagation following distal synaptic activation of hippocampal CA1 pyramidal neurons. Nat Neurosci. 2005; 8:1667–1676. [PubMed: 16299501]

Jensen RJ. Activation of group II metabotropic glutamate receptors reduces directional selectivity in retinal ganglion cells. Brain Res. 2006; 1122:86–92. [PubMed: 17010323]

Johnston D, Hoffman DA, Magee JC, Colbert CM. K+ channel regulation of signal propagation in dendrites of hippocampal pyramidal neurons. Nature. 1997; 387:869–875. [PubMed: 9202119]

Kim JS, Greene MJ, Zlateski A, Lee K, Richardson M, Turaga SC, Purcaro M, Balkam M, Robinson A, Behabadi BF, et al. Space-time wiring specificity supports direction selectivity in the retina. Nature. 2014; 509:331–336. [PubMed: 24805243]

Kingston AE, Ornstein PL, Wright RA, Johnson BG, Mayne NG, Burnett JP, Belagaje R, Wu S, Schoepp DD. LY341495 is a nanomolar potent and selective antagonist of group II metabotropic glutamate receptors. Neuropharmacology. 1998; 37:1–12. [PubMed: 9680254]

Knoflach F, Kemp JA. Metabotropic glutamate group II receptors activate a G protein-coupled inwardly rectifying K+ current in neurones of the rat cerebellum. J Physiol. 1998; 509:347–354. [PubMed: 9575285]

Kosaka T, Tauchi M, Dahl JL. Cholinergic neurons containing GABA-like and/or glutamic acid decarboxylase-like immunoreactivities in various brain regions of the rat. Exp Brain Res. 1988; 70:605–617. [PubMed: 3384059]

Koulen P, Malitschek B, Kuhn R, Wässle H, Brandstätter JH. Group II and group III metabotropic glutamate receptors in the rat retina: distributions and developmental expression patterns. Eur J Neurosci. 1996; 8:2177–2187. [PubMed: 8921309]

Kupferschmidt DA, Lovinger DM. Inhibition of presynaptic calcium transients in cortical inputs to the dorsolateral striatum by metabotropic GABA_B and mGlu2/3 receptors. J Physiol. 2015; 593:2295–2310. [PubMed: 25781000]

Larkum ME, Zhu JJ, Sakmann B. Dendritic mechanisms underlying the coupling of the dendritic with the axonal action potential initiation zone of adult rat layer 5 pyramidal neurons. J Physiol. 2001; 533:447–466. [PubMed: 11389204]

Lee S, Zhou ZJ. The synaptic mechanism of direction selectivity in distal processes of starburst amacrine cells. Neuron. 2006; 51:787–799. [PubMed: 16982423]

Lee S, Kim K, Zhou ZJ. Role of ACh-GABA cotransmission in detecting image motion and motion direction. Neuron. 2010; 68:1159–1172. [PubMed: 21172616]

Lipin MY, Taylor WR, Smith RG. Inhibitory input to the direction-selective ganglion cell is saturated at low contrast. J Neurophysiol. 2015; 114:927–941. [PubMed: 26063782]

Makara JK, Losonczy A, Wen Q, Magee JC. Experience-dependent compartmentalized dendritic plasticity in rat hippocampal CA1 pyramidal neurons. Nat Neurosci. 2009; 12:1485–1487. [PubMed: 19898470]

Miller RF, Bloomfield SA. Electroanatomy of a unique amacrine cell in the rabbit retina. Proc Natl Acad Sci U S A. 1983; 80:3069–3073. [PubMed: 6574470]

Moreno JL, Holloway T, Albizu L, Sealfon SC, González-Maeso J. Metabotropic glutamate mGlu2 receptor is necessary for the pharmacological and behavioral effects induced by hallucinogenic 5-HT2A receptor agonists. Neurosci Lett. 2011; 493:76–79. [PubMed: 21276828]

O'Malley DM, Masland RH. Co-release of acetylcholine and gamma-aminobutyric acid by a retinal neuron. Proc Natl Acad Sci U S A. 1989; 86:3414–3418. [PubMed: 2566171]

Oesch NW, Taylor WR. Tetrodotoxin-resistant sodium channels contribute to directional responses in starburst amacrine cells. PLoS One. 2010; 5:e12447. [PubMed: 20805982]

Otsu Y, Marcaggi P, Feltz A, Isope P, Kollo M, Nusser Z, Mathieu B, Kano M, Tsujita M, Sakimura K, et al. Activity-dependent gating of calcium spikes by A-type K+ channels controls climbing fiber signaling in Purkinje cell dendrites. Neuron. 2014; 84:137–151. [PubMed: 25220810]

Ozaita A, Petit-Jacques J, Völgyi B, Ho CS, Joho RH, Bloomfield SA, Rudy B. A unique role for Kv3 voltage-gated potassium channels in starburst amacrine cell signaling in mouse retina. J Neurosci. 2004; 24:7335–7343. [PubMed: 15317859]

Pei Z, Chen Q, Koren D, Giammarinaro B, Acaron Ledesma H, Wei W. Conditional Knock-Out of Vesicular GABA Transporter Gene from Starburst Amacrine Cells Reveals the Contributions of Multiple Synaptic Mechanisms Underlying Direction Selectivity in the Retina. J Neurosci. 2015; 35:13219–13232. [PubMed: 26400950]

Saugstad JA, Segerson TP, Westbrook GL. Metabotropic glutamate receptors activate G-protein-coupled inwardly rectifying potassium channels in Xenopus oocytes. J Neurosci. 1996; 16:5979–5985. [PubMed: 8815880]

Schoepp DD, Johnson BG, Wright RA, Salhoff CR, Mayne NG, Wu S, Cockerman SL, Burnett JP, Belegaje R, Bleakman D, et al. LY354740 is a potent and highly selective group II metabotropic glutamate receptor agonist in cells expressing human glutamate receptors. Neuropharmacology. 1997; 36:1–11. [PubMed: 9144636]

Seebahn A, Rose M, Enz R. RanBPM is expressed in synaptic layers of the mammalian retina and binds to metabotropic glutamate receptors. FEBS Lett. 2008; 582:2453–2457. [PubMed: 18555800]

Stincic T, Smith RG, Taylor WR. Time course of EPSCs in ON-type starburst amacrine cells is independent of dendritic location. J Physiol. 2016; 594:5685–5694. [PubMed: 27219620]

Taniguchi M, Yokoi M, Shinohara Y, Okutani F, Murata Y, Nakanishi S, Kaba H. Regulation of synaptic currents by mGluR2 at reciprocal synapses in the mouse accessory olfactory bulb. Eur J Neurosci. 2013; 37:351–358. [PubMed: 23167899]

Taylor WR, Vaney DI. Diverse synaptic mechanisms generate direction selectivity in the rabbit retina. J Neurosci. 2002; 22:7712–7720. [PubMed: 12196594]

Tukker JJ, Taylor WR, Smith RG. Direction selectivity in a model of the starburst amacrine cell. Vis Neurosci. 2004; 21:611–625. [PubMed: 15579224]

Vaney DI, Young HM. GABA-like immunoreactivity in cholinergic amacrine cells of the rabbit retina. Brain Res. 1988; 438:369–373. [PubMed: 3345446]

Velte TJ, Miller RF. Spiking and nonspiking models of starburst amacrine cells in the rabbit retina. Vis Neurosci. 1997; 14:1073–1088. [PubMed: 9447689]

Vlasits AL, Morrie RD, Tran-Van-Minh A, Bleckert A, Gainer CF, DiGregorio DA, Feller MB. A Role for Synaptic Input Distribution in a Dendritic Computation of Motion Direction in the Retina. Neuron. 2016; 89:1317–1330. [PubMed: 26985724]

Wei W, Hamby AM, Zhou K, Feller MB. Development of asymmetric inhibition underlying direction selectivity in the retina. Nature. 2011; 469:402–406. [PubMed: 21131947]

van Wyk M, Wässle H, Taylor WR. Receptive field properties of ON- and OFF-ganglion cells in the mouse retina. Vis Neurosci. 2009; 26:297–308. [PubMed: 19602302]

Highlights

- Global dendritic integration improves SAC centrifugal response.
- Electrotonic isolation between dendritic sectors reduces SAC centripetal response.
- mGluR2 signaling restricts cross-compartmental signaling between SAC sectors.
- mGluR2 signaling is important for preferred-direction DSGC spiking at high speed.

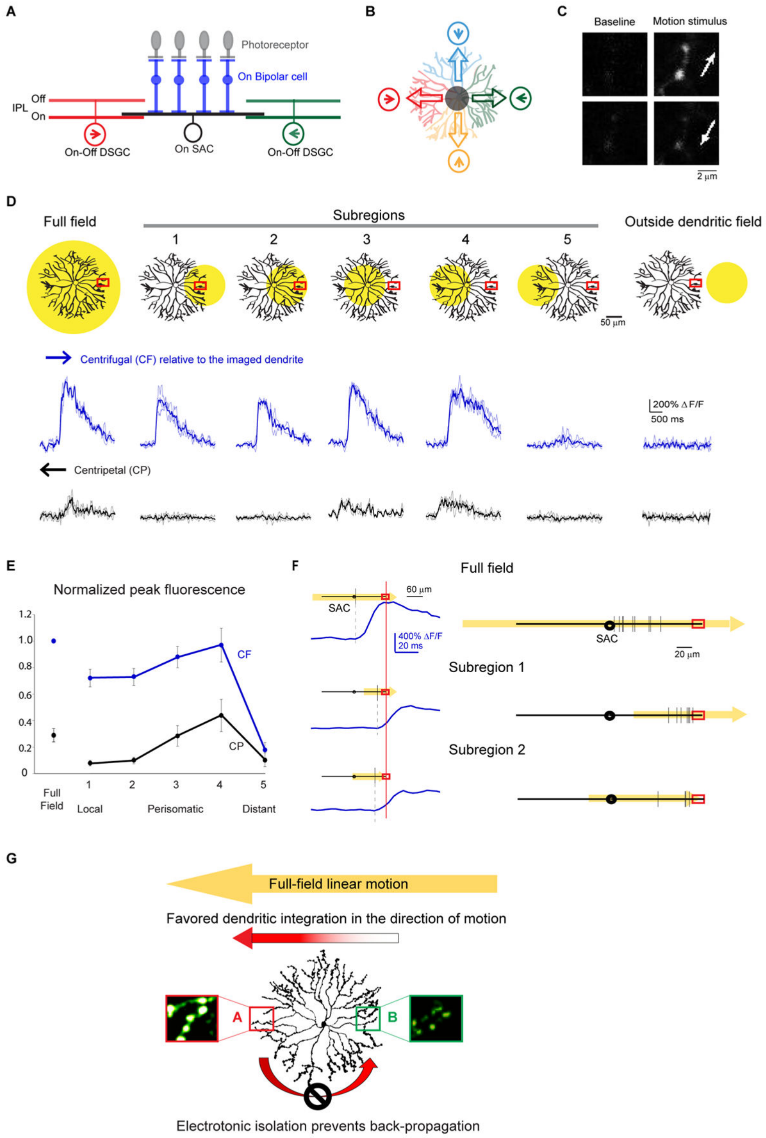

Figure 1. Multiple dendritic compartments contribute to centrifugal direction selectivity of SAC varicosities during linear motion

A. Schematic shows side view of the major cell types and connections involved in the On pathway of the direction selective circuit: the On SAC receives light-driven glutamatergic inputs from On bipolar cells (BP), and sends outputs to On-Off DSGCs. Inhibitory synapses onto a DSGC primarily come from SAC dendritic branches oriented in the null direction of the DSGC. PR: photoreceptor. Arrows indicate the preferred directions of the DSGCs. BP inputs onto the DSGC are not shown for clarity.

B. Schematic of the top view shows the asymmetric inhibition between SACs and DSGCs. Each SAC dendritic quadrant preferentially inhibits a subtype of On-Off DSGC whose preferred direction (arrow in circle) is antiparallel to the orientation of the SAC quadrant. Empty arrows on SAC dendrites indicate the preferred (i.e. centrifugal) directions of the SAC dendritic quadrants.

C. Example images of GCaMP6 fluorescence in distal SAC varicosities of an On SAC from a Chat-IRES-Cre mouse infected with AAV-floxed GCaMP6m at baseline and during the full-field moving bar stimulus in the centrifugal (top) and centripetal (bottom) directions (arrows). Also see Figure S1.

D. Top: Schematics show the SAC dendritic areas within which the moving bar was presented (yellow filled circles) and the location of the calcium imaging window (red rectangles). Bottom: GCaMP6m fluorescence traces during centrifugal (CF) and centripetal (CP) motion under conditions shown at top. CF and CP are relative to the dendrites containing the imaging window. Dark traces represent mean values and light traces represent individual trials. See also Figure S2.

E. Summary graph of peak fluorescence in SAC varicosities in different subregions evoked by motion in the CF and CP directions under the visual stimulus conditions shown in **D**. For each varicosity, responses are normalized to that during full-field motion in the CF direction. For subregion 5, peak amplitude was calculated only from trials that showed detectable responses. CF: full field: 1; subregion 1: 0.71 ± 0.07; subregion 2: 0.72 ± 0.05; subregion 3: 0.87 ± 0.08; subregion 4: 0.96 ± 0.11; subregion 5: 0.17 ± 0.06. CP: full field: 0.27 ± 0.04; subregion 1: 0.07 ± 0.02; subregion 2: 0.10 ± 0.02; subregion 3: 0.28 ± 0.08; subregion 4: 0.43 ± 0.11; subregion 5: 0.10 ± 0.07. n = 6 cells (53 total varicosities) from 6 mice. One-way ANOVA for CF direction: F(5,25) = 54.4, $p < 0.0001$. Tukey's post-hoc tests: Full field vs Subregion 1: p = 0.0015; Full field vs Subregion 2: p = 0.0037; Subregion 1 vs 4: p = 0.019; Subregion 2 vs 4: p = 0.035; Subregion 5 vs all stimuli: $p < 0.0001$. All other comparisons $P > 0.05$. One-way ANOVA for CP direction: F(2,25) = 4.9, p = 0.0029. Tukey's post-hoc tests: Subregion 1 vs 4: p = 0.0048; Subregion 2 vs 4: p = 0.026; Subregion 4 vs 5: p = 0.011. All other comparisons $P > 0.05$.

F. The onset timing of the calcium transients under different stimulus conditions. The dendritic field of the SAC is shown as black lines with the circles in the middle representing somas. The spatial extent and the direction of the moving bar stimuli is shown in yellow. Red rectangles indicate the location of the calcium imaging window. Left: Example calcium responses from one SAC. Vertical black lines on SAC dendrites indicate the spatial position of the moving bar's leading edge when the onset of calcium responses (blue traces) was detected in the varicosity in the imaging window. The calcium traces are aligned in the time axis relative to the time of the moving bar reaching the imaging window (red vertical line). Right: Summary of the onset timing of the calcium responses from multiple cells. Calculated distance from the bar's leading edge to the tip of the imaged dendrite: full field: 77 ± 6 μm, n = 9 cells; subregion 1: 18 ± 3 μm, n = 8 cells; subregion 2: 25 ± 8 μm, n = 4 cells. One-way ANOVA F(2,18) = 38.8, $p < 0.0001$. Tukey's post-hoc: Full field vs subregion 1: p = 0.0001; Full field vs subregion 2: p = 0.0001; subregion 1 vs subregion 2: p = 0.72.

G. A model of SAC dendritic processing during full-field linear motion. Sequential activation of SAC dendritic tree from right to left leads to strong centrifugal response in location A due to efficient spatiotemporal summation of depolarization along the motion trajectory. However, the strong centrifugal response in A does not propagate efficiently back to B due to electronic isolation between SAC dendritic branches.

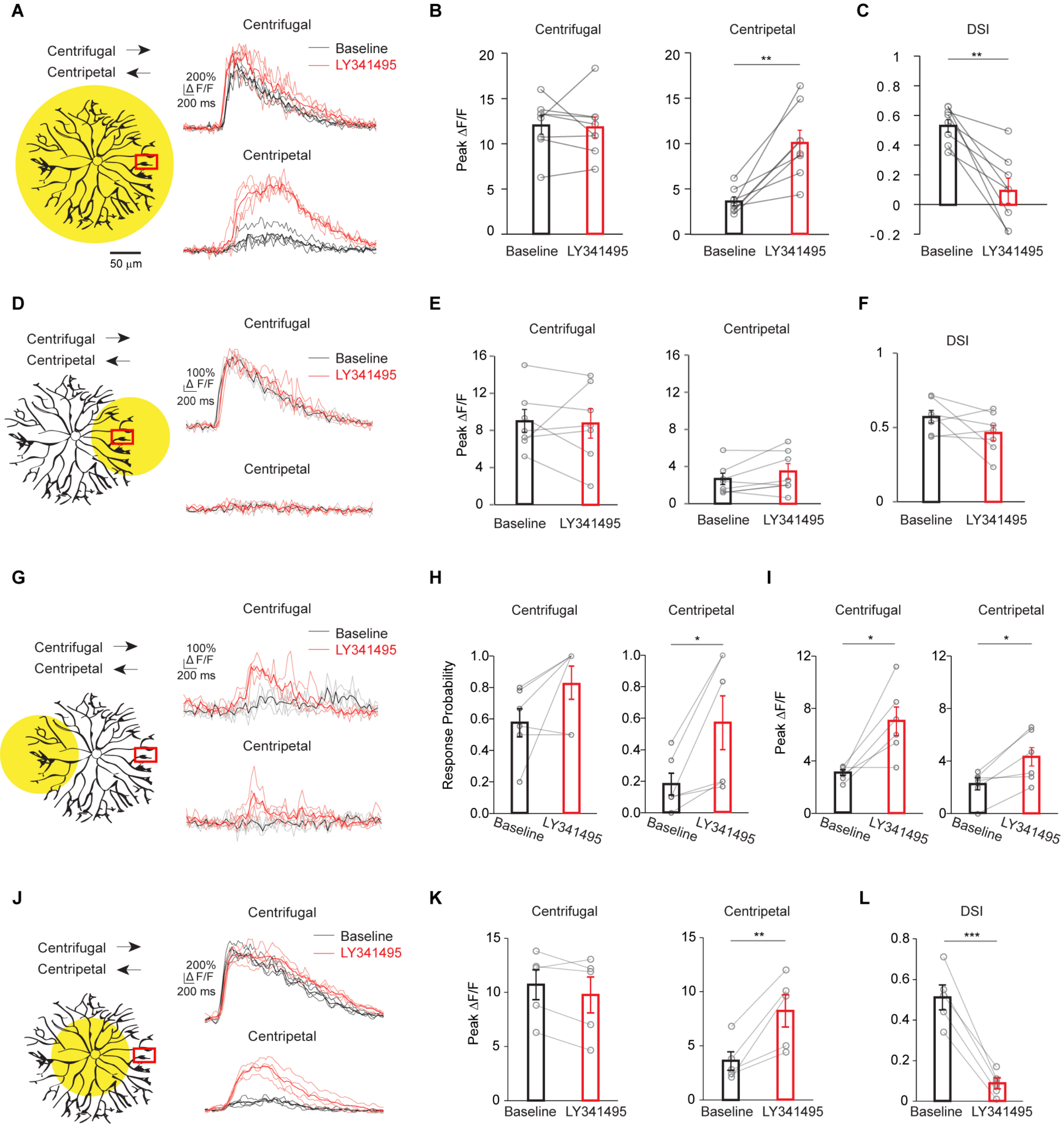

Figure 2. mGluR2 signaling promotes electrotonic isolation of SAC dendritic branches

A – C. mGluR2 blockade selectively increases centripetal-direction response during full field linear motion. See also Figure S3.

A. Left: same as full-field stimulus in Figure 1D, schematic shows the spatial extent of the motion stimulus and the location of the calcium imaging window. Arrows indicate motion directions. Right: GCaMP6M fluorescence traces under this stimulus condition before (black) and after adding LY341495 (red). Dark traces represent mean values and light traces represent individual trials for **A**, **D**, **G** and **J**.

B. Summary of peak fluorescence of individual SACs before and after adding LY341495 under the condition shown in **a**. Centrifugal: baseline, 12.1 ± 1.0; LY341495, 11.8 ± 1.2; p = 0.80. Centripetal: baseline, 3.6 ± 0.5; LY341495, 10.1 ± 1.4; **p = 0.0018. n = 8 cells (97 varicosities) from 7 mice.

C. Same as **B**, summary of direction selectivity index (DSI) values. Baseline, 0.54 ± 0.04; LY341495, 0.09 ± 0.08; **p = 0.0016.

D – F. mGluR2 blockade has no effect on the SAC calcium response when the motion stimulus is restricted to the local dendritic branches containing the imaging window.

D. Left: schematic same as subregion 1 in Figure 1D. Right: GCaMP6M fluorescence traces of a varicosity before (black) and after adding LY341495 (red).

E. Summary of peak fluorescence of individual SACs before and after adding LY341495 under the condition shown in **D**. Centrifugal: baseline, 8.9 ± 1.3; LY341495, 8.8 ± 1.6; p = 0.88. Centripetal: baseline, 2.6 ± 0.6; LY341495, 3.5 ± 0.8; p = 0.17. n = 7 cells (57 varicosities) from 6 mice.

F. Same as **e**, summary of DSI values. Baseline, 0.57 ± 0.04; LY341495, 0.46 ± 0.05; p = 0.15.

G – I: mGluR2 blockade enhances the calcium response of SAC varicosities when the motion stimulus is restricted to the dendritic sector located opposite the imaging window.

G. Left: schematic same as subregion 5 in Figure 1D. Right: GCaMP6M fluorescence traces under the stimulus condition shown on the left.

H. Summary of the response probability during motion in the centrifugal and centripetal directions under the stimulus condition shown in **G**. Response probability is calculated as the number of trials with detectable calcium responses divided by the total number of trials (See Methods). Centrifugal: baseline, 0.55 ± 0.09; LY341495, 0.83 ± 0.11; p = 0.097. Centripetal: baseline, 0.17 ± 0.07; LY341495, 0.64 ± 0.14; *p = 0.02. n = 6 cells (53 varicosities) from 6 mice.

I. As in **G**, summary of peak amplitude of the propagated responses. Peak amplitude is calculated only from the trials with detectable calcium responses. Centrifugal: baseline, 3.0 ± 0.2; LY341495, 7.0 ± 1.1; *p = 0.016. Centripetal: baseline, 2.2 ± 0.5; LY341495, 4.3 ± 0.8; *p = 0.018.

J – L: mGluR2 blockade enhances centripetal-direction responses of SAC varicosities during perisomatic motion stimulation.

J. Left: schematic same as subregion 3 in Figure 1D. Right: GCaMP6M fluorescence traces under the stimulus condition shown on the left.

K. Summary of peak fluorescence of individual SACs before and after adding LY341495 during perisomatic stimulation (data combined for subregions 3 and 4 in Figure 1D). Centrifugal: baseline, 10.7 ± 1.4; LY341495, 9.8 ± 1.7; p = 0.13. Centripetal: baseline, 3.6 ± 0.9; LY341495, 8.2 ± 1.5; *p = 0.01. n = 5 cells (39 varicosities) from 5 mice.

L. Same as **K**, summary of DSI values. Baseline, 0.51 ± 0.06; LY341495, 0.09 ± 0.03; ***p = 0.0001.

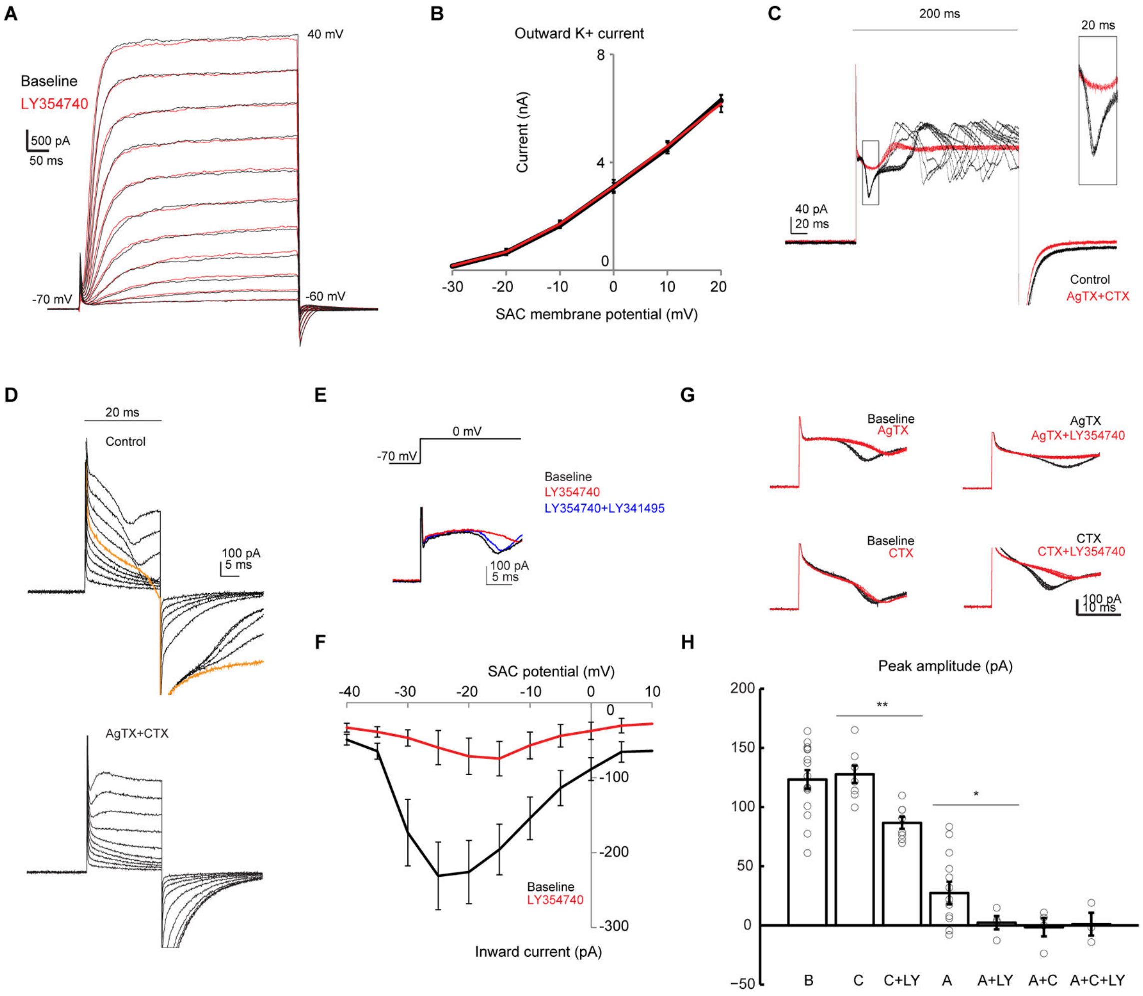

Figure 3. mGluR2 inhibits voltage-gated calcium channels, but not voltage-gated potassium channels in SACs

A. Voltage clamp traces of a SAC in potassium-based internal solution during steps of depolarization at 10 mV increment before (black) and after adding the mGluR2 agonist LY354740 (red).

B. Relationship between average steady-state outward potassium current and membrane potential in SACs before (black) and after LY354740 (red). Repeated measures ANOVA $p = 0.49$, $n = 4$ cells from 3 mice.

C. Example voltage clamp traces of a SAC in cesium-based internal solution at baseline and after addition of AgTX and CTX (AgTX + CTX) during steps of depolarization from −70 mV to 0 mV for 200 ms. For each condition, traces represent the overlay of 10 repetitions. Capacitive currents are clipped for clarity for **C**, **D** and **E**. Inset shows the boxed region at higher magnification.

D. Example voltage clamp traces of a SAC at the baseline (upper), and after addition of AgTX and CTX (lower) during steps of 20 ms depolarization from −70 mV at 10 mV increment. Orange trace represents the onset of the inward calcium transient.

E. Example voltage clamp traces of a SAC at the baseline, and after sequential addition of LY354740 and then the competitive antagonist LY341495 (LY354740 + LY341495).

F. Relationship between peak of the inward current and membrane potential in SACs before and after LY354740. Repeated measures ANOVA **p = 0.0017, n = 9 cells from 5 mice.

G. Example traces of the same SACs before (black) and after (red) application of selective calcium antagonist and LY354740. For each condition, traces represent the overlay of 10 repetitions.

H. Summary of effects of CTX (C), AgTX (A) and LY354740 (LY) on the peak amplitude of the initial calcium transient. Baseline, 123.4 ± 7.8, n = 14 cells from 6 mice; C, 127.7 ± 7.3, n = 8 cells; C + LY, 86.7 ± 5.1, n = 8 cells; A, 27.4 ± 9.5, n = 14 cells; A + LY, 2.3 ± 5.6, n = 4 cells; A + C, −1.5 ± 7.7, n = 4 cells; A + C + LY, 1.1 ± 9.7, n = 3 cells; C versus C + LY, **p = 0.0006; A versus A + LY, * p = 0.02.

See also Figure S4.

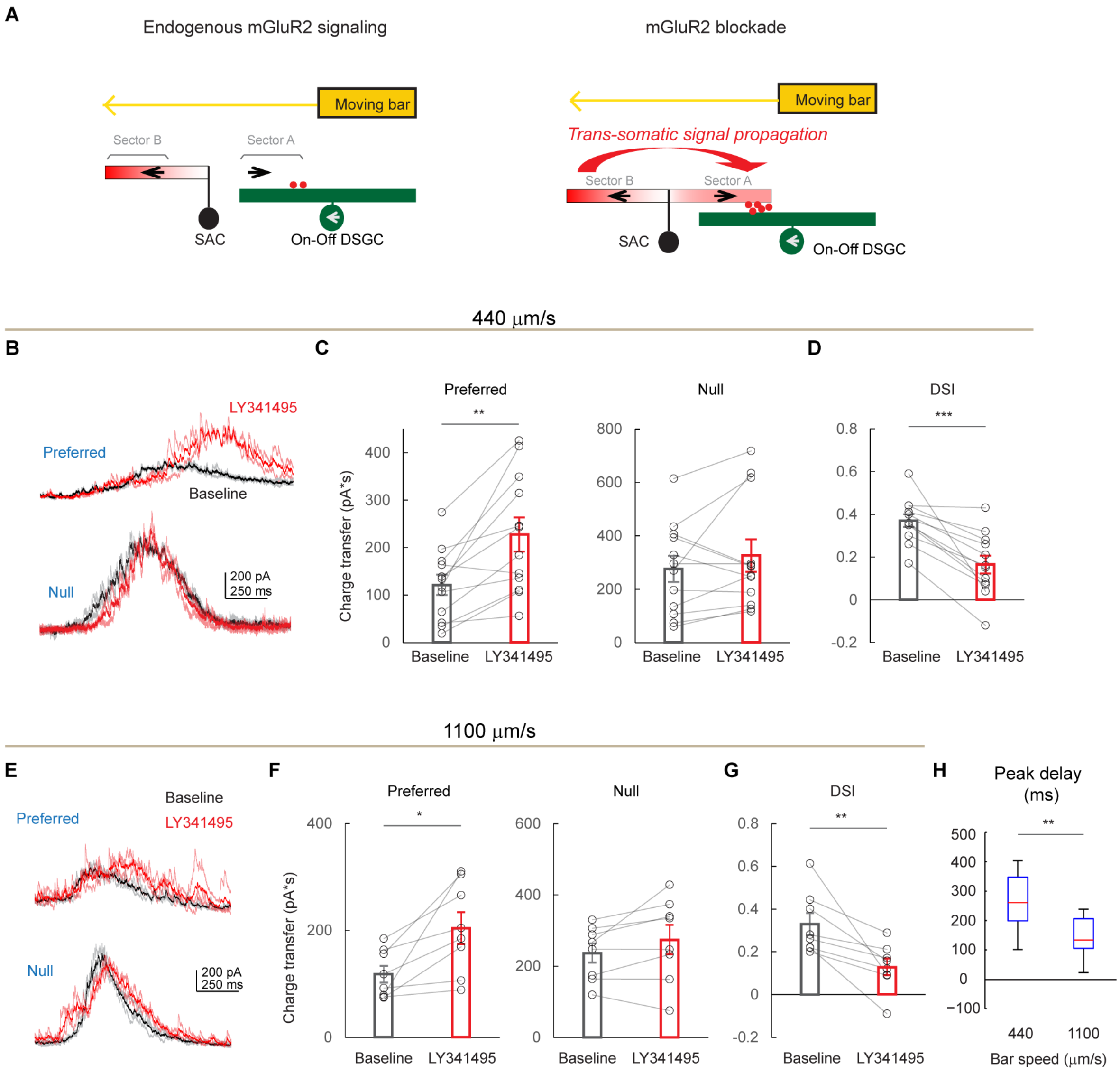

Figure 4. mGluR2 blockade causes an enhanced but delayed preferred-direction inhibition onto DSGCs

A. A model of mGluR2-dependent dendritic compartmentalization in SACs. Left: During endogenous mGluR2 signaling, SAC dendritic branches are more isolated from each other. A bar moving in the preferred direction of the DSGC (leftward) triggers minimal GABA release (red dots) from the centripetally activated sector A of the SAC. Subsequent activation of sector B in the centrifugal direction does not propagate efficiently to sector A to trigger GABA release. Right: During mGluR2 blockade, electrotonic isolation between SAC branches is reduced. Therefore, the strong centrifugal response of sector B propagates more efficiently to sector A. This leads to enhanced dendritic activation of sector A and more GABA release onto the DSGC during motion in the DSGC’s preferred direction.

B – D. DSGC IPSCs before and after adding LY341495 at the bar speed of 440 μm/s.

B. Example On components of IPSC traces of DSGCs in a wild type mouse evoked by a dark bar moving in the preferred and null directions at a bar speed of 440 μm/s before (black) and after (red) adding LY341495. Dark traces represent mean values and light traces represent individual trials. Also see Figures S5B–S5D for IPSC data evoked by a bright bar.

C. Summary of charge transfer of IPSCs in the preferred and null directions at the speed of 440 μm/s in wild type mice. Preferred: baseline, 121.8 ± 21.6 pA·s; LY341495, 227.5 ± 36.0 pA·s; **p = 0.002. Null: baseline, 275.9 ± 48.9 pA·s; LY341495, 325.7 ± 60.8 pA·s; p = 0.23. n = 12 cells from 5 mice. Also see Figures S5B–S5D.

D. As in **C**, summary of DSI values for IPSCs in wild type mice at the bar speed of 440 μm/s. Baseline, 0.37 ± 0.03; LY341495, 0.17 ± 0.04; *** p = 0.0001.

E – G. DSGC IPSCs before and after adding LY341495 at the bar speed of 1100 μm/s.

E. As in **B**, example IPSC traces of DSGCs at the bar speed of 1100 μm/s.

F. As in **C**, summary of charge transfer of IPSCs at the bar speed of 1100 μm/s. Preferred: baseline, 118.0 ± 15.8 pA·s; LY341495, 204.6 ± 29.9 pA·s; *p = 0.01. Null: baseline, 236.9 ± 26.8 pA·s; LY341495, 274.1 ± 41.1 pA·s; p = 0.13. n = 8 cells from 5 mice.

G. As in **D**, summary of DSI values for IPSCs at the bar speed of 1100 μm/s. Baseline, 0.33 ± 0.05; LY341495, 0.13 ± 0.04; ** p = 0.008.

H. Boxplot of the temporal delay of IPSC peak due to LY341495 application in wild type mice at the bar speed of 440 um/s and 1100 um/s. Mean ± SEM: 440 um/s, 289 ± 39 ms; 1100 um/s, 147 ± 20 ms; **p = 0.005. n = 12 cells from 7 mice. Also see Figure S5A.

Also see Figure S6 for the effect of LY341495 on DSGCs from mGluR2 KO mice and alpha RGCs.

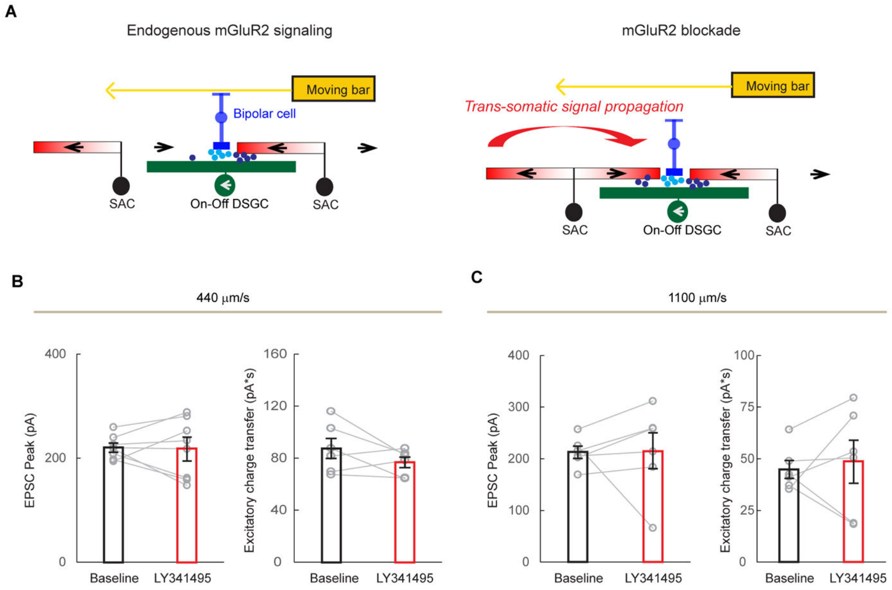

Figure 5. mGluR2 blockade does not significantly change preferred-direction excitation onto DSGCs

A. A model of the effect of mGluR2 blockade on DSGC excitation. The total excitation comes from two sources: glutamate (light blue dots) released from bipolar cells and acetylcholine (dark blue dots) from SACs. SACs form cholinergic synapses with DSGCs in an isotropic pattern. During mGluR2 blockade, enhanced trans-somatic propagation of depolarization in SACs causes increased acetylcholine release only from the centripetally activated SAC sectors, but not from centrifugally activated sectors. The glutamate release is not affected. Therefore, in contrast to the inhibitory inputs, the effect of mGluR2 blockade on the overall excitatory inputs is less pronounced. Also see Discussion.

B. Summary of EPSC peak amplitude and charge transfer in the preferred direction at the speed of 440 μm/s before and after adding LY341495. Peak: baseline, 220.2 ± 8.9; LY341495, 217.4 ± 22.8; p = 0.89, n = 7 cells from 5 mice. Charge transfer: baseline, 87.5 ± 7.8; LY341495, 76.8 ± 4.0; p = 0.19.

C. Summary of EPSC peak amplitude and charge transfer in the preferred direction at the speed of 1100 μm/s before and after adding LY341495. Peak: baseline, 212.2 ± 11.8; LY341495, 215.5 ± 34.8; p = 0.93, n = 6 cells from 4 mice. Charge transfer: baseline, 44.8 ± 4.3; LY341495, 48.5 ± 10.4; p = 0.70.

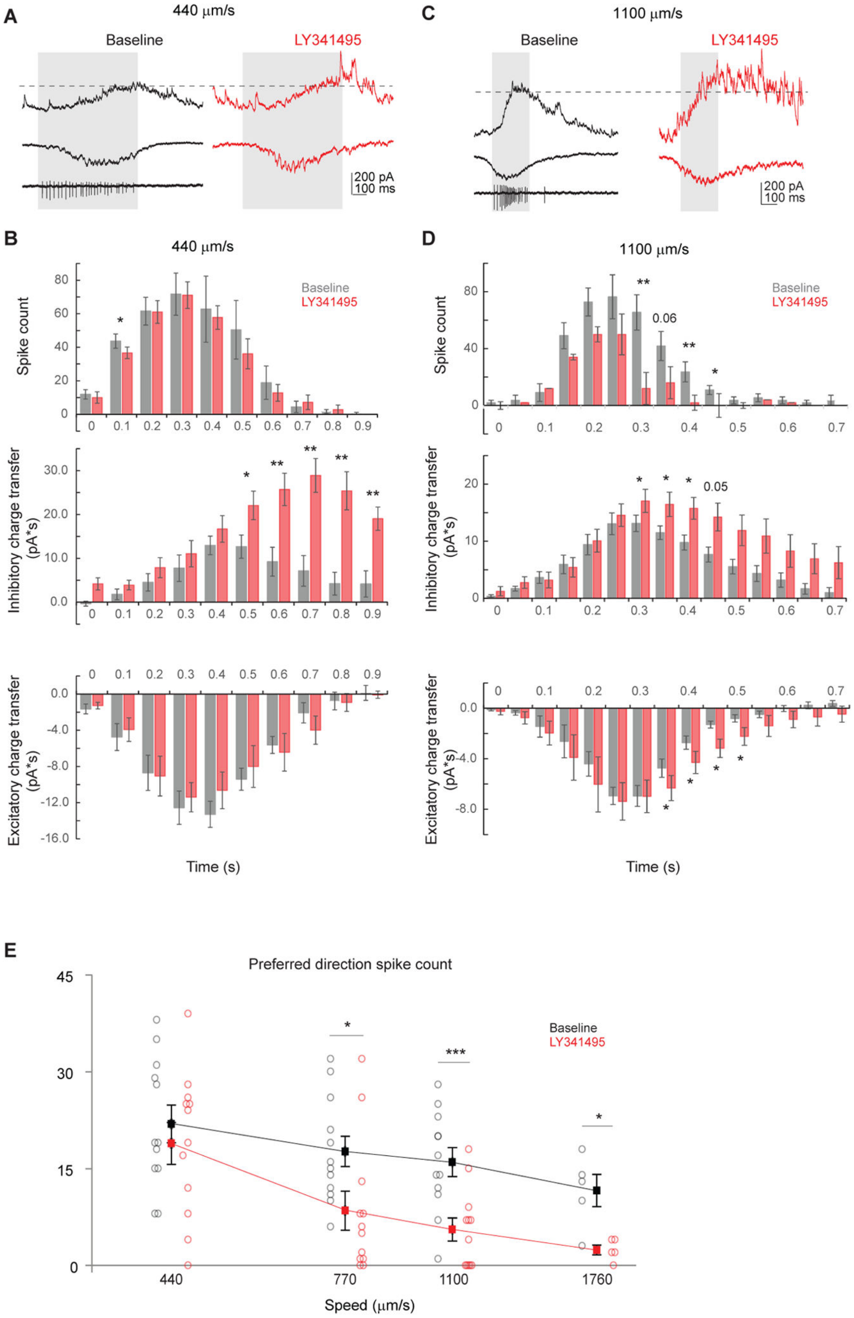

Figure 6. mGluR2 blockade decreases preferred-direction spiking of DSGCs at higher bar speed

A. Example loose cell-attached and whole-cell recordings of a DSGC showing IPSC (upper), EPSC (middle) and spiking (lower left) in the baseline condition (left) and the IPSC and EPSC from the same cell after adding LY341495 (right) evoked by a bar moving in the preferred direction at the bar speed of 440 μm/s. Shaded area represents the temporal window of spiking activity at the baseline condition. Dashed line indicates the peak IPSC level at baseline condition. The LY341495-enhanced IPSC component lags behind spiking activity.

B. Summary histograms of DSGC spike count (upper), inhibitory charge transfer (middle) and excitatory charge transfer (lower) before and after adding LY341495 at the speed of 440 μm/s. Spiking: n = 9 cells; inhibition: n = 6 cells; excitation: n = 6 cells. Spiking: 0.1 – 0.2 s: *p = 0.02. Inhibition: 0.5 – 0.6 s: *p = 0.035; 0.6 – 0.7 s: **p = 0.004; 0.7 – 0.8 s: **p = 0.003; 0.8 – 0.9 s: **p = 0.005; 0.9 – 1.0 s: **p= 0.003.

C. As in **A**, example loose cell-attached and whole-cell recordings of a DSGC showing IPSC (upper), EPSC (middle) and spiking (lower left) in the baseline condition (left) and the IPSC and EPSC from the same cell after adding LY341495 (right) evoked by a bar moving in the preferred direction at the bar speed of 1100 μm/s. A portion of he LY341495-enhanced IPSC component coincides with spiking activity.

D. As in **B**, summary histograms of DSGC spike count (upper), inhibitory charge transfer (middle) and excitatory charge transfer (lower) before and after adding LY341495 at the speed of 440 μm/s. Spiking: n = 11 cells; inhibition: n = 8 cells; excitation: n = 8 cells. Spiking: 0.30–0.35 s: **p = 0.001; 0.40 – 0.45 s: *p = 0.008; 0.45 – 0.50 s: *p = 0.015. Inhibition: 0.30 – 0.35 s: *p = 0.029; 0.35 – 0.40 s: *p = 0.023; 0.40 – 0.45 s: *p = 0.019. Excitation: 0.35 – 0.40 s: * p = 0.037; 0.40 – 0.45 s: *p = 0.042; 0.45 – 0.50 s: *p = 0.015; 0.50 – 0.55 s: *p = 0.049.

E. Summary plot of preferred direction spike count before and after adding LY341495 at different speeds. Horizontal (speed) axis is in log scale. Mean ± SEM: 440 μm/s: baseline, 21.9 ± 2.9; LY341495, 18.9 ± 3.2; p = 0.42, n = 12 cells; 770 μm/s: baseline, 17.7 ± 2.9; LY341495, 8.5 ± 3.0; *p = 0.035, n = 12 cells; 1100 μm/s: baseline, 16.0 ± 2.2; LY341495, 5.6 ± 1.8; *** p = 0.0001, n = 12 cells; 1760 μm/s: baseline, 11.6 ± 2.5; LY341495, 2.4 ± 0.7; *p = 0.01, n = 5 cells

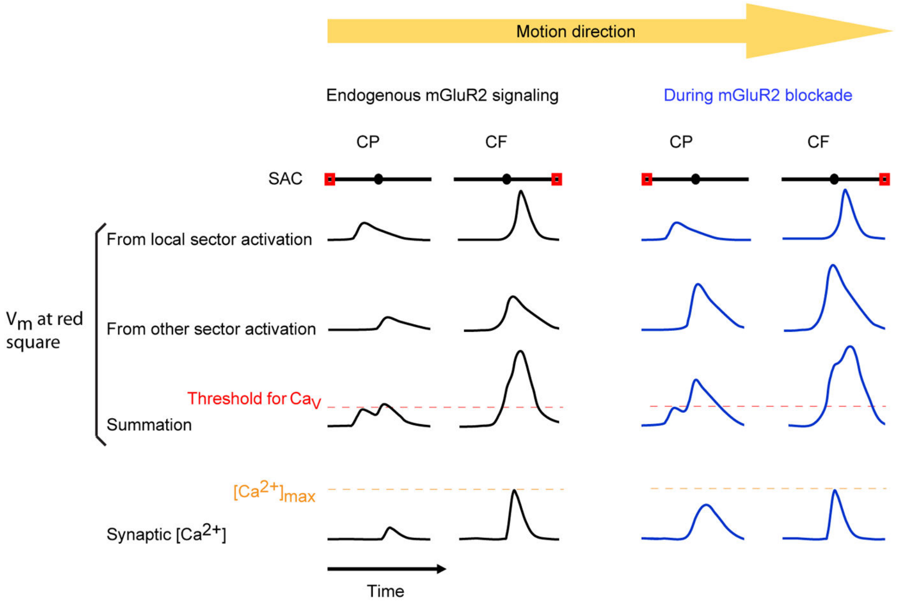

Figure 7. A model of the effect of mGluR2 blockade on SAC dendritic activation during full field motion

The dendritic field of the SAC is shown as black lines with the circles in the middle representing somas. The traces represent the Vm or calcium response over time at the varicosities indicated by red rectangles. Vm from local sector activation refers to the membrane depolarization caused by activation of only the dendritic sector containing the red square. mGluR2 blockade does not affect the component of depolarization from local sector activation (see Figure **2D–2F**). Vm from other sector activation refers to membrane depolarization at the red square caused by activation of the rest of the dendritic tree, which is enhanced by mGluR2 blockade (see Figure **2G–2I**). Vm summation refers to the arithmetic sum of the responses from local sector and other sector stimulation. The threshold for voltage-dependent Ca^{2+} channel activation is shown as red dashed line. Synaptic $[Ca^{2+}]$ saturates at the level indicated by the orange dashed line. CF calcium response is saturated at the varicosities and therefore cannot be further enhanced by mGluR2 blockade.